ISSN 1392-1207. MECHANIKA. Vol. 31, No. 3, 2025: 243–250

Investigation on Energy Output Performance of IPMC Optical-Controlled Composite Driving Based on PLZT Ceramic

Yafeng LIU*,*,****, Xiaole MA**, Pingmei MING***, Jianhui CHEN****, Xuejie LIANG*****

*School of Mechanical and Electrical Engineering, Henan University of Technology, Zhengzhou 450001, China, E-mail: yfliu@haut.edu.cn (Corresponding Author)

**School of Mechanical and Electrical Engineering, Henan University of Technology, Zhengzhou 450001, China, E-mail: lantern2213@stu.haut.edu.cn

***School of Mechanical and Power Engineering, Henan Polytechnic University, Jiaozuo 454003, China, E-mail: mingpingmei@163.com

****Shitai Industrial Corp Ltd., Taizhou 317100, China, E-mail: chenjianhui@shitai.com.cn

*****School of Mechanical and Electrical Engineering, Henan University of Technology, Zhengzhou 450001, China, E-mail: 19522290336@163.com

https://doi.org/10.5755/j02.mech.40175

1. Introduction

Ionic Polymer-Metal Composite (IPMC) possesses outstanding flexibility, low driving voltage (<5 V), high power efficiency, and biocompatibility, making it suitable for soft mechatronics and robotics applications, particularly in flexible sensing and actuation. However, electroactive driven IPMC can be influenced by electromagnetic interference in complex environments, which leads to its limitations in practical application. PLZT ceramic, a functional photovoltaic ceramic material, exhibits remarkable electromechanical coupling properties. When PLZT ceramic is exposed to UV light, it can provide a stable driving source for IPMC through its own intrinsic photoelectric conversion mechanism, effectively overcome the performance fluctuations caused by unstable external power supplies or electromagnetic interference, and ensure the stability and reliability of the driving process. Therefore, the IPMC driving method under the excitation of light source has great application potential, and is expected to provide more reliable and efficient driving and energy output solutions for future flexible electronic devices and bionic robots.

In view of the excellent characteristics of IPMC, scholars have actively explored the application of IPMC in different fields and achieved remarkable results. In the field of biomimetic robotics, researchers have developed various biomimetic systems using IPMC. For instance, Safari et al. [1] had proposed and developed a cost-effective robotic fish using IPMC artificial muscle and wireless solar charging technology for monitoring aquatic pollution. Wang et al. [2] designed electromagnetically controlled millirobots inspired by carpenter ants. Using wireless power transmission and an IPMC gripper, these robots can manipulate small components individually or in pairs. Carrico et al. [3] from the University of Utah created an IPMC-based biomimetic caterpillar robot with the help of 3D printing technology. He et al. [4] combined the characteristics of tulips with those of IPMC to successfully simulate the blooming process of bionic tulips, providing new ideas for biological behavior simulation and biomimetic robot development. Zhao et al. [5] integrated IPMC with the flapping-wing principle of the biomimetic beetle to innovatively propose a new type of flapping-wing micro air vehicle. Li et al. [6] ingeniously designed a capsule-shaped underwater robot by leveraging the properties of IPMC. Zhang et al. [7] designed and manufactured a biomimetic butterfly soft robot driven by Ag-IPMC. In the medical field, Chang et al. [8] developed a polydimethylsiloxane-based drug depot integrated with IPMC actuators, enabling drug release in an aqueous environment upon wireless activation, thus revolutionizing the drug release technology. Brunetto et al. [9] proposed an IPMC-based vibrotactile probe for biomedical detection. Ming et al. [10] integrated IPMC sensors into smart gloves to monitor human activities. Cheong et al. [11] designed wireless-powered IPMC microgrippers for non-destructive grasping of fish eggs. Wang et al. [12] proposed the design of a drug dual-chamber valveless delivery pump using IPMC and adopted an adaptive control scheme. Mousavi et al. [13] designed a remotely controlled drug delivery implantable chip, using IPMC as the moving cover of the reservoir, and tested its performance and biocompatibility.

Regarding PLZT ceramic research, Lee et al. [14] prepared PLZT ceramic with good transparency and piezoelectric properties and used them to fabricate fully transparent piezoelectric speakers capable of outputting sounds in different frequency ranges under specific voltages, meeting the requirements of next-generation transparent electronic devices. Chen et al. [15] prepared transparent PLZT fiber by extrusion technology and used them to make high-frequency ultrasonic transducers, demonstrating their imaging capabilities through object imaging. Geng et al. [16] prepared highly optically transparent original PLZT and Ni-doped PLZT ceramic with bandgap engineering and first used them as self-powered photodetectors, showing high detection rates and fast response times under specific light conditions. Vandana et al. [17] prepared flexible PVDF/PLZT composite films by solution casting technology and studied the influence of PLZT ceramic content on film properties, determining its importance in thermal and mechanical energy harvesting. Wang et al. [18] proposed a photo-induced ion drag pump based on PLZT ceramic. The performance of the pump can be enhanced by optimizing the electrode structure, fluid channel and increasing the light intensity, providing a design guideline for its applications in microfluidics, soft robots and heat

dissipation of micro devices. Qi et al. [19] theoretically designed and numerically studied a silicon/PLZT hybrid microring modulator based on the silicon-on-insulator (SOI) platform, which has potential application value in optical communication. Yue et al. [20] proposed a non-contact shape adjustment method of PLZT photovoltaic-driven PVDF based on the photovoltaic effect and inverse piezoelectric effect. The effectiveness was verified by modeling and experiments, and the application directions were pointed out. Tang et al. [21] proposed a novel photo-electrostatic hybrid-driven micromirror based on the anomalous photovoltaic effect of PLZT ceramic. Rahman [22] studied the lateral deflection of PLZT photodriver cantilevers under different conditions using a light chopper based on the photostrictive effect of PLZT films on silicon wafers. Chen et al. [23] prepared a high-performance self-powered ultraviolet photodetector based on the ZnO/PLZT heterojunction by coupling the ferroelectric depolarization field and the built-in potential of the heterojunction. Zhang et al. [24] developed PLZT-TENG using antiferroelectric ceramic with large polarization differences and proposed a method to improve the output performance of triboelectric nanogenerators through the polarization of inorganic ceramic dielectrics. Chen et al. [25] synthesized PLZT films by a low-cost sol-gel method and developed a self-powered ultraviolet photodetector with an Au/PLZT/FTO structure. Liu et al. [26] proposed a new closed-loop control method with a switching control strategy based on PLZT ceramic photo actuators.

Despite extensive research on the photo-induced characteristic of PLZT ceramic as energy conversion components, studies on the IPMC composite driving energy output performance under PLZT ceramic configuration remain limited. Most of the existing theoretical models primarily focus on the individual performance of either PLZT ceramic or IPMC material itself, and the output energy performance of IPMC composite driving under the excitation of light source is still relatively scarce. In this paper, based on the IPMC optical-controlled composite driving method [27], an energy output model is constructed. Then, for IPMC of different sizes, the corresponding parameters such as driving force and deformation are obtained by using different voltages and light intensities as excitation sources, and on this basis, the energy output analysis is carried out to improve the previous research on the composite driving theory.

2. Model Analysis

2.1. Electrical model of optical-controlled IPMC composite driving method

When PLZT ceramic is exposed to UV light, a series of complex photoelectric physical processes occur internally, generating photocurrent between the electrodes. The electrical model of PLZT ceramic can be equivalently represented as a circuit composed of a constant current source. In this model, there is a parallel connection of resistor R_P and capacitor C_P, while the resistor R_1 and capacitor C_1 are connected in parallel at both ends of PLZT ceramic. Therefore, the equivalent electrical model is depicted in Fig. 1.

The driving voltage of this equivalent circuit model is given by:

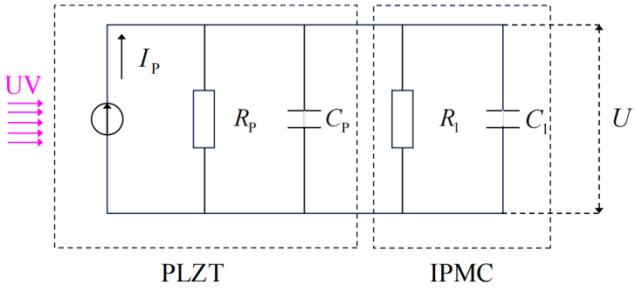

Fig. 1 Equivalent electrical model

$$U = I_P \frac{R_P R_1}{R_P + R_1}\left(1 - e^{-\frac{t}{\tau'}}\right) = U_s'\left(1 - e^{-\frac{t}{\tau'}}\right), \tag{1}$$

where I_P represents the constant current source current, U_s' represents the photogenerated voltage, and τ' represents the time constant, which can respectively be expressed as:

$$U_s' = I_P \frac{R_P R_1}{R_P + R_1}, \tag{2}$$

$$\tau' = \frac{R_P R_1}{R_P + R_1}\left(C_P + C_1\right). \tag{3}$$

2.2. Deformation output model of IPMC

When PLZT ceramic is illuminated by high-energy UV light, the photocurrent voltage is generated within the material. The IPMC load mechanism can be simplified to a cantilever beam fixed at one end and subjected to uniformly distributed loads. The specific mechanical simplification is shown in Fig. 2, L is the length of the cantilever beam AB, q is the distributed force, and θ is the torsion angle.

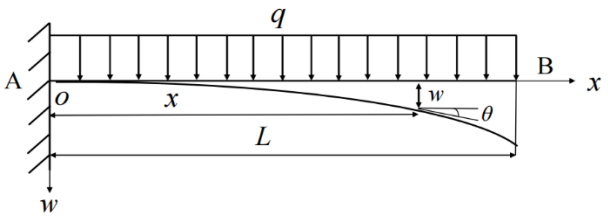

Fig. 2 Simplified mechanical model of IPMC load mechanism

The angle equation and deflection equation of the driving model can be obtained:

$$\theta(x) = -\frac{q}{6EI}\left[(L-x)^3 - L^3\right], \tag{4}$$

$$w(x) = \frac{q}{24EI}\left[(L-x)^4 + 4L^3 x - L^4\right]. \tag{5}$$

Further simplifying to a cantilever beam model subjected to tip load F_0 and bending moment M_0, as illustrated in Fig. 3.

The maximum deflection angle and maximum output deformation related to the photovoltage can be ex-

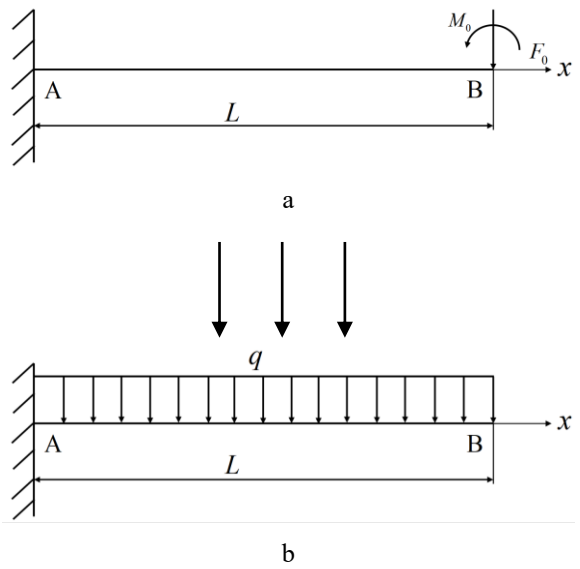

Fig. 3 Equivalent mechanical model of IPMC load mechanism: a – mechanical model of cantilever beam subjected to uniformly distributed load, b – mechanical model of cantilever beam with free - end subjected to tip load and bending moment

pressed as:

$$w_{\max} = \frac{\alpha L^3}{3EI}\left(1 - e^{-\frac{t}{\tau'}}\right)U_s', \tag{6}$$

$$\theta_{\max} = \frac{4\alpha L^2}{9EI}\left(1 - e^{-\frac{t}{\tau'}}\right)U_s', \tag{7}$$

where α is the proportionality coefficient, EI is the flexural rigidity of the IPMC, t is the driving time.

2.3. Energy output model

To thoroughly study the energy output characteristic of IPMC composite driving method, the output energy E of each IPMC under voltage excitation is defined. The output energy represents the cumulative effect of the output force acting on objects in space, and its magnitude is equal to the product of the output force and the output deformation. Thus, the formula can be derived as:

$$E = F \times w, \tag{8}$$

where F is the output force of the IPMC, and w is the maximum output deformation at the end of material.

3. Experimental Investigation and Analysis

3.1. Overview of the experimental setup and objectives

To verify the energy output characteristic of IPMC under the configuration of PLZT ceramic, a series of tests were conducted to examine the energy output performance of IPMC under direct current and light excitation. The variation trend of IPMC output energy is measured with different IPMC dimensions, DC voltage and light intensity as variables.

In this work, the metallic electrode layers of the IPMC are composed of platinum (Pt), which offers low surface resistance and stable performance. IPMC samples of varying lengths—20 mm, 30 mm, 40 mm, and 50 mm—are selected and designated as 20-IPMC, 30-IPMC, and so on, respectively. All samples have a width of 5 mm and a thickness of 0.2 mm, as illustrated in Fig. 4. The dimensional parameters of the PLZT ceramic are 10 mm × 5 mm × 0.8 mm (length × width × thickness).

Fig. 4 IPMC samples

Through the experimental platform, deformation and driving force were tested and analyzed under both DC power supply and light excitation. In the DC electrical experiments, the input voltage value was incrementally adjusted, and the energy output changes of IPMC with different dimensions were observed and recorded. For the light driving test, the intensity of light was varied, and similarly, the energy output conditions of IPMC with different dimensions were recorded.

3.2. Experiments under direct current driving

For the DC driving test, an experimental setup is established as depicted in Fig. 5. A multi-channel function generator capable of producing signals ranging from 0.1 Hz to 10 MHz at voltages between 0 and 20 V is utilized. The measuring range of the strain gauge sensor is ±15mm and the detection accuracy is 30 μm. The deformation of IPMC is indirectly reflected by measuring the strain generated during the driving process. The data acquisition card has the function of eight-channel single-end input, which can connect multiple sensors at the same time to realize

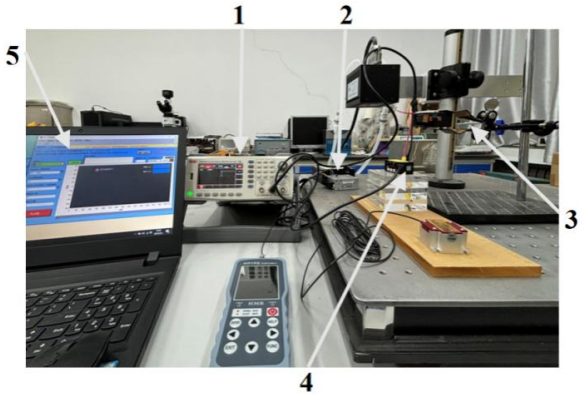

Fig. 5 Diagram of the DC driving experimental setup:
1 – data acquisition module, *2* – specialized fixture, *3* – displacement sensor, *4* – signal generator, *5* – computer

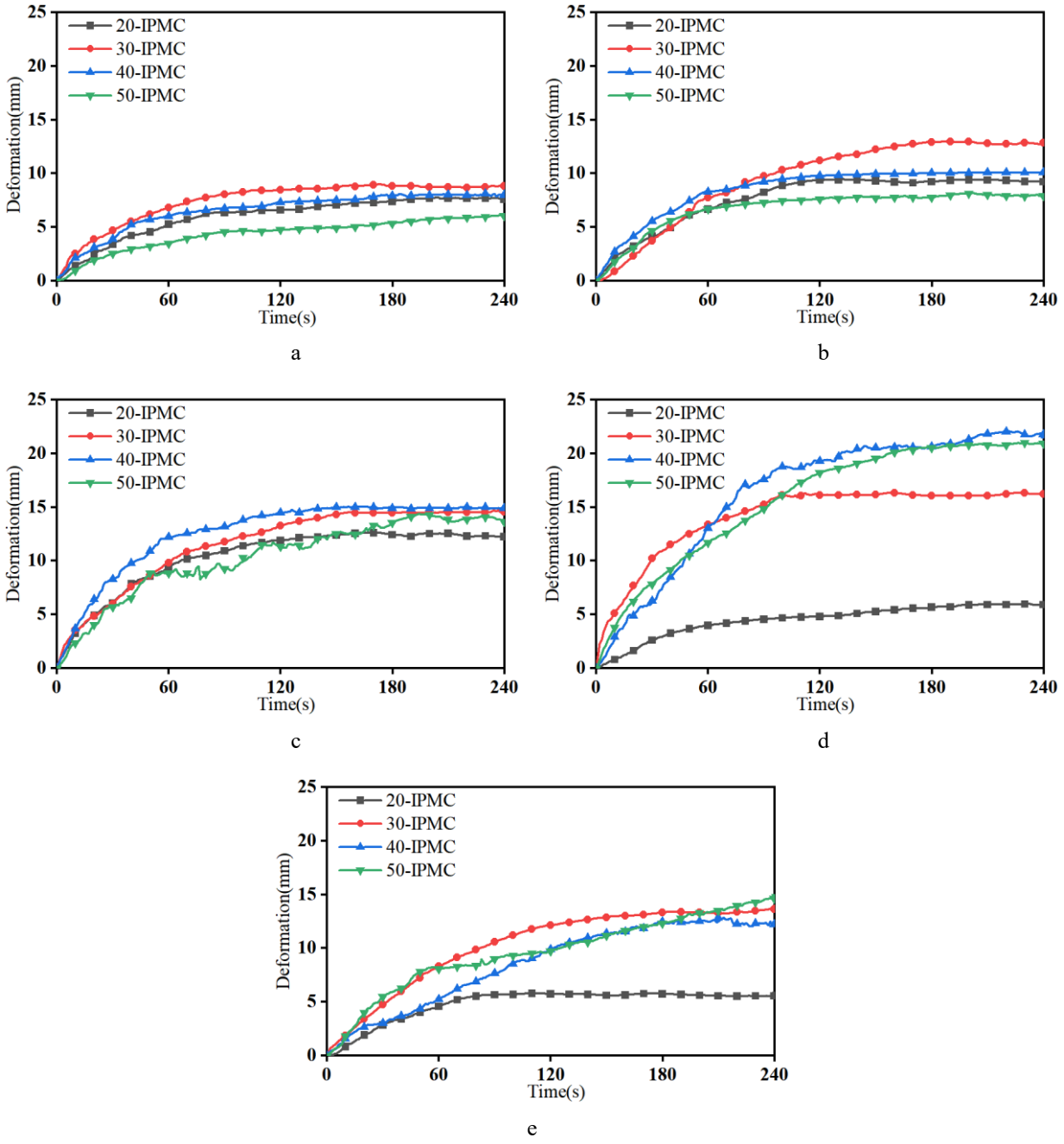

Fig. 6 Deformation curves of various IPMC sizes under different voltages: a – 2 V, b – 2.5 V, c – 3 V, d – 3.5 V, e – 4 V

synchronous acquisition of multiple physical quantities. Each IPMC sample is securely fastened to a custom fixture. In this experiment, the function generator outputs 2 ~ 4V DC as the input driving signal of IPMC. The output strain of IPMC is measured by the strain gauge sensor in real time, and the measured data is collected by the data acquisition card, and transmitted to the computer for analysis and processing. After each experiment, IPMC is immersed in water for 5-10 minutes to maintain its hydration level and ensure accurate results for subsequent test.

Deformation curves for IPMC of varying sizes at different voltages are depicted in Fig. 6. It can be observed that all IPMC samples exhibit similar trends under identical voltage conditions. Within a 240-second timeframe, the output deformation increased over time until it stabilized. This trend indicates a good response characteristic of the IPMC to applied voltage. As shown in Fig. 6, d, when the driving voltage is 3.5 V, the maximum output deformation of all IPMC samples is achieve, with relatively steady changes and minimal fluctuation. Notably, the 40-IPMC reaches its peak output deformation after 125 seconds, providing significant deformation in the initial phase, which is about 20 to 40 seconds faster than the 20-IPMC and 50-IPMC, respectively.

From the above experimental results, different sizes of IPMC exhibit similar performance characteristics for a given voltage input. In the experiment, the 40-IPMC can not only achieve a large output deformation, but also has a faster response speed, and maintain a relatively stable output characteristics throughout the experiment period.

As shown in Fig. 7, it describes the output force of IPMC of the same size under different voltages. From Fig. 7, it can be observed that all sizes of IPMC follow an identical gain pattern: as the voltage increases, the output

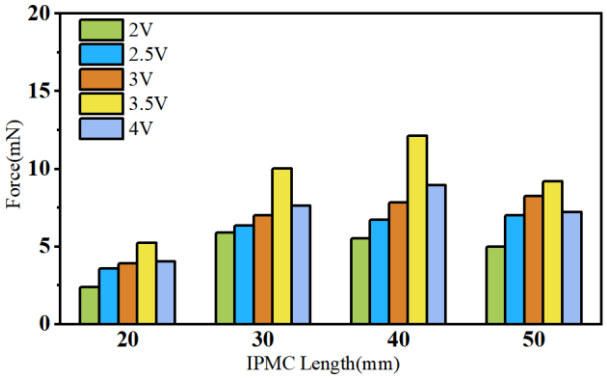

Fig. 7 Output force of identical IPMC sizes under varying voltages

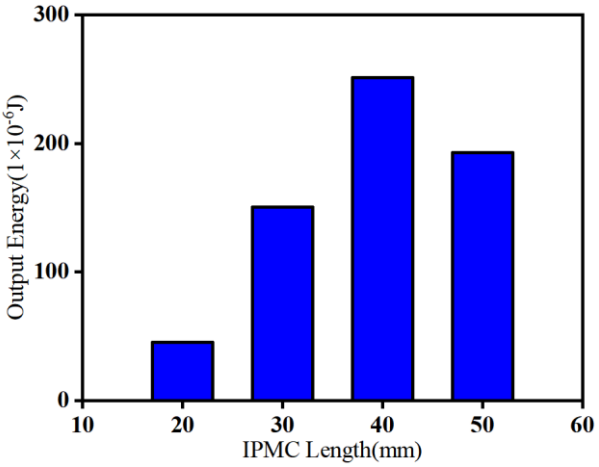

Fig. 8 Energy output of various IPMC sizes under DC electric driving

force of the IPMC significantly rises until reaching a saturation point. When the input voltage is gradually increased from 2 V to 3.5 V, the output force of the same-sized IPMC continuously climbs, reaching its maximum value at 3.5 V. Compared to other sizes, the driving force of the 40-IPMC is notably enhanced. The comprehensive study of the driving force of IPMC of different sizes indicates that the change trends are consistent with the characterization results of output deformation.

As illustrated in Fig. 8, it shows the output energy of IPMC of different sizes driven by DC power. From Fig. 8, it can be seen that when the input voltage is 3.5 V, each size of IPMC has reached its respective maximum output force. Under this voltage excitation condition, the output energy of the 40-IPMC is significantly higher than that of other size IPMC. Moreover, the 40-IPMC demonstrates greater output deformation, faster response speed, and longer stable operating time, further validating the superior output performance of the 40-IPMC under 3.5 V voltage excitation.

3.3. Experiments under UV light driving

To investigate the energy output performance of IPMC optical-controlled composite driving method, an experimental setup is constructed as illustrated in Fig. 9. High-energy UV light source irradiates the PLZT ceramic surface vertically, the generated photovoltage is measured by a high-impedance voltmeter sensor and the transmitted to the voltmeter controller and finally to the computer for

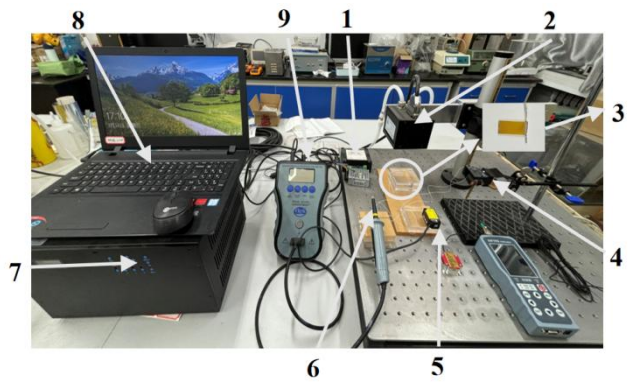

Fig. 9 Diagram of the optical driving experimental setup: *1* – data acquisition module, *2* – light source, *3* – PLZT ceramic, *4* – specialized fixture, *5* – displacement sensor, *6* – high-resistance voltmeter sensor head, *7* – UV light source controller, *8* – computer, *9* – high-resistance electrostatic voltmeter

processing. After each test, IPMC is again hydrated to prevent dehydration-induced performance degradation.

The photovoltaic voltage graphs for PLZT ceramic under UV light intensities of 150 μW/cm², 300 μW/cm² and 600 μW/cm² are shown in Fig. 10. The UV light intensity significantly affects the photovoltaic voltage of the PLZT ceramic; higher intensity yields higher photovoltaic voltage. With increasing light intensity, the saturation value of photovoltaic voltage increased rapidly, reaching saturation points of 3 V, 3.5 V and 4 V respectively. Higher light intensities lead to saturation value of photovoltaic voltage, faster response time and shorter duration to reach saturation.

The output deformation curves for differently sized IPMC under uniform light intensity are presented in Fig. 11. Over 240 seconds, all curves show the consistent deformation trend: the driving voltage increases with the increase of light intensity, and the output deformation gradually increases before stabilizing. In terms of response rate, the output deformation of IPMC of all sizes experiences rapid growth, slow down and steady state. Specifically, under light intensity of 300 μW/cm², all PLZT samples reach their maximum output deformation within 90 to 120 seconds, which demonstrates rapid response capability. In this experiment, the 40-IPMC shows the largest output deformation and fastest response compared to other sizes at the same light intensity.

Fig. 12 depicts the output force of IPMC of the same size under different light intensities. As the light intensity increases, the driving force of IPMC shows a noticeable enhancement trend. When the input light intensity rises from 150 μW/cm² to 600 μW/cm², the output force of the same size of IPMC continuously increases, indicating that the light-controlled IPMC exhibits high sensitivity and good response characteristics to UV light excitation. At an input light intensity of 300 μW/cm², each size of the IPMC reaches its maximum output force, with the 40-IPMC demonstrating more stable driving force, which indicates that under different light intensities, the driving force and output deformation of IPMC exhibit similar change trends.

Fig. 13. presents the energy output of IPMC of different sizes under light driving. When the light intensity is 300 μW/cm², the output motion performance of IPMC is

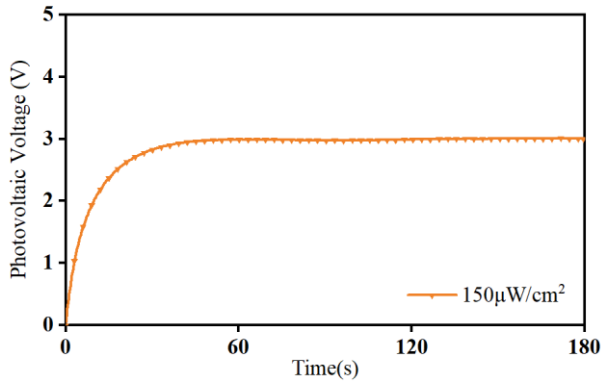

a

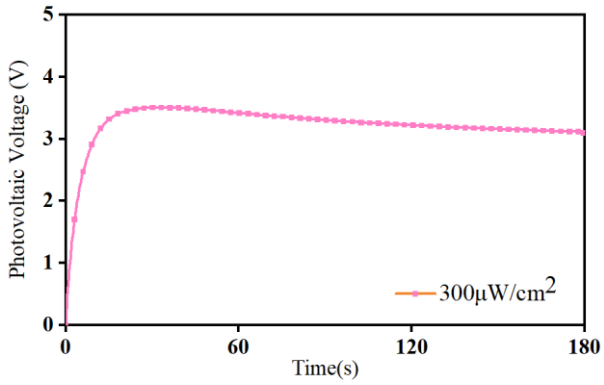

b

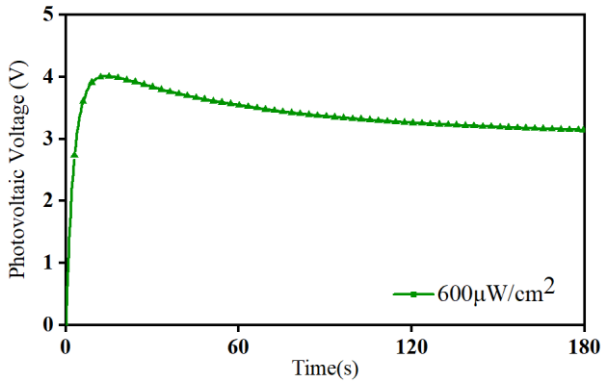

c

Fig. 10 Photovoltage graph under different light intensities: a – 150 μW/cm², b – 300 μW/cm², c – 600 μW/cm²

optimal. From the output deformation and output force results, the energy output conditions of different sizes of IPMC under light excitation are shown in the energy diagram. As depicted in Fig. 13, the energy output of 40-IPMC is significantly higher than that of other sizes, highlighting its superior performance under the light intensity of 300 μW/cm².

In summary, it can be seen from the driving force and energy output experimental results of IPMC optical-controlled composite driving that IPMC of different sizes presents similar changing trends under different light intensity. At the same time, the experimental results of IPMC driven by light and direct current show a high degree of consistency, verifying that IPMC driven by light also has good driving force and energy output characteristics.

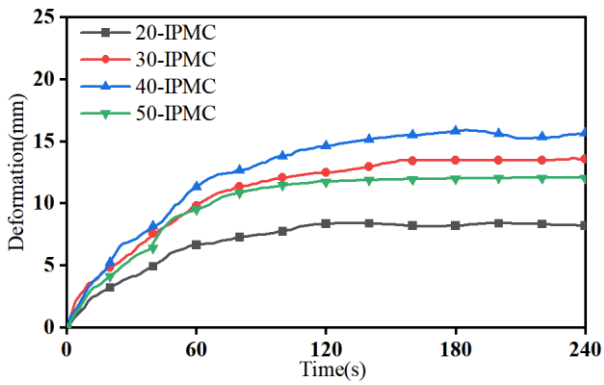

a

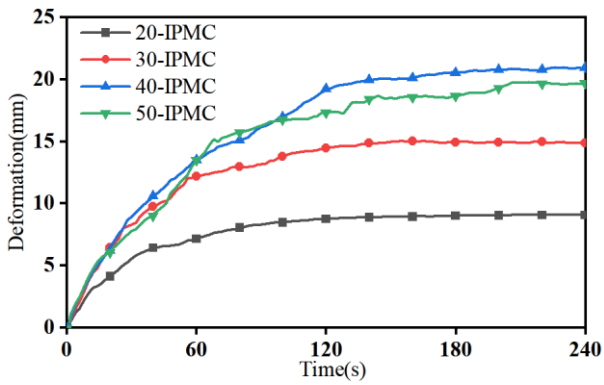

b

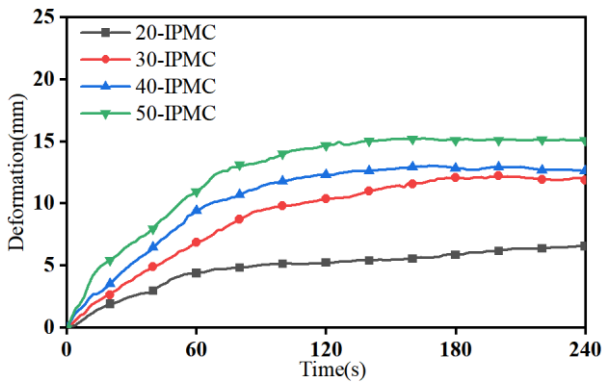

c

Fig. 11 Deformation curves of various IPMC sizes under the same light intensity: a – 150 μW/cm², b – 300 μW/cm², c – 600 μW/cm²

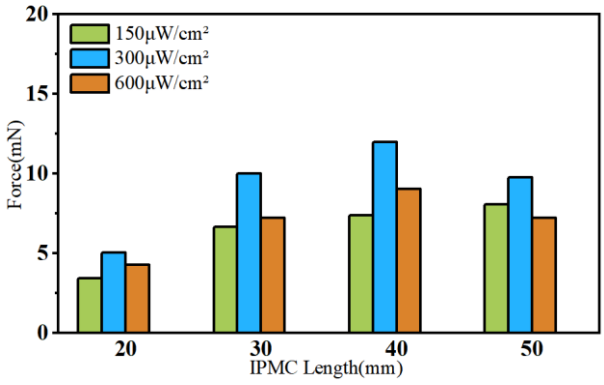

Fig. 12 Output force of identical IPMC sizes under different light intensities

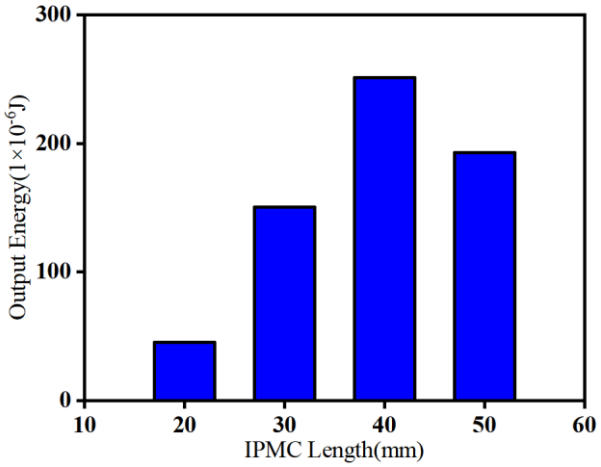

Fig. 13 Energy output of various IPMC sizes under light excitation

4. Conclusions

Based on the previously proposed IPMC optical-controlled composite driving method that utilizes the photoelectric characteristic of PLZT ceramic, this study further deepened the understanding of this innovative driving approach, the energy output model of IPMC driven by light source is established, and the driving force and energy output are analyzed through a series of experiments. The results show that compared with the traditional direct current drive method, under different light intensity conditions, the IPMC driven by light source can not only respond faster and reach a stable output state, the change trend of its driving force is consistent with the change trend of output deformation, but also shows good energy output characteristic, which further verifies the rationality and accuracy of the proposed IPMC optical-controlled composite driving method. This study not only improves the IPMC optical-controlled composite driving theory based on PLZT ceramics, but also provides a guiding basis for the wide application of this drive method, and is expected to promote the development of intelligent driving system to a higher level.

Acknowledgments

This work is supported by the National Natural Science Foundation of China (No. 52405101) and the Foundation of Henan University of Technology (No. 2021BS064).

References

1. **Safari, Y.; Naghavi, N.; Malayjerdi, M.; Kalani, H.** 2022. Design and test of wirelessly powered IPMC artif icial muscle for aquatic ecosystem health applications, Journal of Intelligent Material Systems and Structures 33(16): 2074-2085. https://doi.org/10.1177/1045389X211072522.
2. **Wang, J.; Jiao, N.; Tung, S.; Liu, L.** 2019. Target clamping and cooperative motion control of ant robots, Bioinspiration & Biomimetics 14(6): 066015. https://doi.org/10.1088/1748-3190/ab4839.
3. **Carrico, J. D.; Leang, K. K.** 2017. Fused filament 3D printing of ionic polymer-metal composites for soft robotics, In Proc. SPIE 10163, Electroactive Polymer Actuators and Devices (EAPAD) 2017, 10163: 70-82. https://doi.org/10.1117/12.2259782.
4. **Tian, A.; Wang, X.; Sun, Y.; Zhang, X.; Wang, H.; Yang, L.** 2021. Preparation and performance analysis of Pt-IPMC for driving bionic tulip, Journal of Advanced Dielectrics 11(4): 2150017. http://doi.org/10.1142/S2010135X2150017X.
5. **Zhao, Y.; Xu, D.; Sheng, J.; Meng, Q.; Wu, D.; Wang, L.; Xiao, J.; Lv, W.; Chen, Q.; Sun, D.** 2018. Biomimetic Beetle-Inspired Flapping Air Vehicle Actuated by Ionic Polymer-Metal Composite Actuator, Applied Bionics and Biomechanics 2018(1): 3091579. https://doi.org/10.1155/2018/3091579.
6. **Li, H.; Fan, M.; Yue, Y., Hu, G.; He, Q.; Yu, M.** 2020. Motion control of capsule-like underwater robot utilizing the swing properties of ionic polymer metal composite actuators, Journal of Bionic Engineering 17(2): 281-289. https://doi.org/10.1007/s42235-020-0022-7.
7. **Zhang, L.; Ren, J.; Tian, A.; Li, J.; Chen, Q.; Wang, Y.; Du, H.** 2024. Study on surface morphology and properties of biological type Ag-IPMC and its application on butterfly soft robot, Ceramics International 50(23): 52075-52081. https://doi.org/10.1016/j.ceramint.2024.04.114.
8. **Chang, X. L.; Chee, P. S.; Lim, E. H.; Chong, W. C.** 2019. Radio-frequency enabled ionic polymer metal composite (IPMC) actuator for drug release application, Smart Materials and Structures 28(1): 015024. https://doi.org/10.1088/1361-665X/aaefd3.
9. **Brunetto, P.; Fortuna, L.; Giannone, P.; Graziani, S.; Pagano, F.** 2010. A Resonant Vibrating Tactile Probe for Biomedical Applications Based on IPMC. IEEE Transactions on Instrumentation and Measurement 59(5): 1453-1462. https://doi.org/10.1109/TIM.2009.2038297.
10. **Ming, Y.; Yang, Y.; Fu, R. P.; Lu. C.; Zhao. L.; Hu. Y. M.; Li. C.; Wu. Y. X.; Liu, H.; Chen, W.** 2018. IPMC Sensor Integrated Smart Glove for Pulse Diagnosis, Braille Recognition, and Human–Computer Interaction, Advanced Materials Technologies 3(12): 1800257. https://doi.org/10.1155/2018/3091579.
11. **Cheong, H. R.; Teo, C. Y.; Leow, P. L.; Lai, K. C.; Chee, P. S.** 2018. Wireless-powered electroactive soft microgripper, Smart Materials and Structures 27(5): 055014. https://dx.doi.org/10.1088/1361-665X/aab866.
12. **Wang, J.; McDaid, A. J.; Lu, C. Z.; Aw, K. C.** 2017. A Compact Ionic Polymer-Metal Composite (IPMC) Actuated Valveless Pump for Drug Delivery, IEEE/ASME Transactions on Mechatronics 22(1): 196-205. https://doi.org/10.1109/TMECH.2016.2624762.
13. **Mousavi, M. M. S.; Karami, A. H.; Ghasemnejad, M.; Kolahdouz, M.; Manteghi, F.; Ataei, F. 2**018. Design of a remote-control drug delivery implantable chip for cancer local on demand therapy using ionic polymer metal composite actuator, Journal of the Mechanical Behavior of Biomedical Materials 86: 250-256. https://doi.org/10.1016/j.jmbbm.2018.06.034.
14. **Lee, Y.; Choi, H.; Jang, J.** 2025. Fabrication and characterization of lead lanthanum zirconate titanate ceramic-based fully transparent piezoelectric loud-

speakers for next-generation electronic devices, Sensors and Actuators A: Physical 382: 116087. https://doi.org/10.1016/j.sna.2024.116087.
15. **Chen, X.; Chen, R.; Chen, Z.; Chen, J.; Shung, K. K.; Zhou, Q.** 2016. Transparent lead lanthanum zirconate titanate (PLZT) ceramic fibers for high-frequency ultrasonic transducer applications, Ceramics International 42(16): 18554-18559. https://doi.org/10.1016/j.ceramint.2016.08.195.
16. **Geng, H.; Xiao, H.; Lin, G.; Zhong, H.; Cheng, H.; Shi, Z.; Guo, Y.** 2020. Visible or near-infrared light self-powered photodetectors based on transparent ferroelectric ceramics, ACS Applied Materials & Interfaces 12(30): 33950-33959. https://doi.org/10.1021/acsami.0c09991.
17. **Vandana; Tomar, M.; Gupta, R.** 2023. Thermal and mechanical energy harvester based on flexible PVDF/PLZT polymer-ceramic composites, Journal of Polymer Research 30(8): 330. https://doi.org/10.1007/s10965-023-03694-7.
18. **Wang, X.; Lv, Z.; Shao, Y.; Shi, Y.; Yao, Y.; Wang, J.** 2024. Investigation on Influence Factors of Photo-Induced PLZT-Based Ion Drag Pump, Micromachines 15(12): 1424. https://doi.org/10.3390/mi15121424.
19. **Qi, Z.; Hu, G.; Liu, C.; Li, L.; Yun, B.; Zhang, R.; Cui, Y.** 2017. Design and investigation of a novel silicon/ferroelectric hybrid electro-optical microring modulator, Optics Communications 385: 130-135. https://doi.org/10.1016/j.optcom.2016.10.050.
20. **Yue, H. H.; Jiang, J.; Long, Y. F.; Song, Y. J.** 2014. Modelling and experiments of PLZT/PVDF hybrid drive method for non-contact shape adjustment, International Journal of Applied Electromagnetics and Mechanics 46(4): 867-877. https://doi.org/10.3233/JAE-140095.
21. **Tang, Y. J.; Chen, Y. S.; Qiao, K.; Wang, X. J.** 2018. Micro-mirror with hybrid photoelectric-electrostatic driving of PLZT ceramic, IOP Conference Series: Materials Science and Engineering 307(1): 012016. https://doi.org/10.1088/1757-899X/307/1/012016.
22. **Rahman, M.; Ahmed, M.; Nawaz, M.; Molina, G.; Rahman, A.** 2017. Experimental Investigation of Photostrictive Materials for MEMS Application, Open Access Library Journal 4(11): 1-23. https://doi.org/10.4236/oalib.1103856.
23. **Chen, J.; Wang, Z.; He, H.; Mao, J.; Zhang, Y.; Zhang, Q.; Li, M.; Lu, Y.; He, Y.** 2021. High-Performance Self-Powered Ultraviolet Photodetector based on Coupled Ferroelectric Depolarization Field and Heterojunction Built-In Potential, Advanced Electronic Materials 7(12): 2100717. https://doi.org/10.1002/aelm.202100717.
24. **Zhang, J.; Zhang, Y.; Sun, N.; Li, Y.; Du, J.; Zhu, L.; Hao, X.** 2021. Enhancing output performance of triboelectric nanogenerator via large polarization difference effect, Nano Energy 84: 105892. https://doi.org/10.1016/j.nanoen.2021.105892.
25. **Chen, J.; Priya, A. S.; You, D.; Pei, W.; Zhang, Q.; Lu, Y.; Li, M.; Guo, J.; He, Y.** 2020. Self-driven ultraviolet photodetectors based on ferroelectric depolarization field and interfacial potential, Sensors and Actuators A: Physical 315: 112267. https://doi.org/10.1016/j.sna.2020.112267.
26. **Liu, Y.; Yang, Y.; Liu, C.; Wang, X.** 2023. An ON-OFF Closed-Loop Control of Photoelectric Actuator Based on PLZT Ceramic, Mechanika 29(6): 530-538. https://doi.org/10.5755/j02.mech.33716.
27. **Liu, Y.; Ming, P.; Chen, J.; Jing, C.** 2024. Experimental Analysis of IPMC Optical-Controlled Flexible Driving Performance under PLZT Ceramic Configuration, Sensors 24(17): 5650. https://doi.org/10.3390/s24175650.

Y. Liu, X. Ma, P. Ming, J. Chen, X. Liang

INVESTIGATION ON ENERGY OUTPUT PERFORMANCE OF IPMC OPTICAL-CONTROLLED COMPOSITE DRIVING BASED ON PLZT CERAMIC

S u m m a r y

Ionic polymer-metal composite (IPMC), as an intelligent material, exhibits advantages such as rapid responsiveness, large deformation angles, and high flexibility, leading to its extensive application in biomimetic machinery, biomedicine and other fields. In this paper, based on the previous proposed IPMC optical-controlled composite driving method under lanthanum-modified lead zirconate titanate (PLZT) ceramic configuration, the output energy characteristic is analyzed by establishing a novel model and conducting a series of experiments. The analysis and experimental results show that under different light intensities, the driving force and output deformation of IPMC with varying dimensions exhibit similar trends, both increasing gradually and reach a maximum value. Furthermore, the deformation curves of IPMC driven by light source are consistent with those driven by direct current, confirming that IPMC under light excitation also possesses stable and excellent energy output properties. Therefore, the research on the energy output of IPMC optical-controlled composite driving not only provides deeper theoretical guidance for its application in flexible driving area, but also promotes the vigorous development of IPMC in other innovative technological fields.

Keywords: IPMC, PLZT ceramic, optical-controlled composite driving, energy output.

Received January 14, 2025
Accepted June 25, 2025